J. Fluid Mech. (2007), *vol.* 592, *pp.* 495–505.
doi:10.1017/S0022112007008634 Printed in the United Kingdom

Optimal growth of the Batchelor vortex viscous modes

C. J. HEATON

Department of Applied Mathematics and Theoretical Physics, University of Cambridge, Wilberforce Road, Cambridge CB3 0WA, UK

(Received 15 June 2007 and in revised form 10 September 2007)

We present calculations of optimal linear growth in the Batchelor (or q) vortex. The level of transient growth is used to quantify the effect of the viscous centre modes found at large Reynolds number and large swirl. The viscous modes compete with inviscid-type transients, which are seen to provide faster growth at short times. Following a smooth transition, the viscous modes emerge as dominant in a different regime at later times. A comparison is drawn with two-dimensional shear flows, such as boundary layers, in which weak instability modes (Tollmien–Schlichting waves) also compete with inviscid transients (streamwise streaks). We find the competition to be more evenly balanced in the Batchelor vortex, because the inviscid transients are damped faster in a swirling jet than a two-dimensional shear flow, so that despite their weak growth rates the viscous modes may be relevant in some situations.

1. Introduction

High-Reynolds-number vortices have been a focus of hydrodynamic stability theory ever since the work of Rayleigh. Isolated vortices are experimentally observed to be unstable in many configurations (Leibovich 1978), but the mathematical description of vortex breakdown is still far from complete. Applications for vortex stability theory range from tornadoes to swirling pipe flow and even fully developed turbulence, but in this paper we concentrate on the vortex derived by Batchelor (1964) to model a trailing line vortex. The stability of the trailing line vortex is of importance in aeronautics as the vortex poses a hazard on runways.

Our mean flow, the Batchelor vortex, is described by a single parameter q which measures the swirl strength. There is a large literature documenting the stability of this flow for different values of q and Reynolds number Re. Values of $q \geqslant 2$ are of the most practical interest (Leibovich 1978), but for these values the observed instability of the vortex is not yet fully understood. The documented instabilities fall into three broad categories.

(a) Exponential instability modes of an inviscid nature (meaning that the exponential growth rate increases to a finite value as $Re \to \infty$). These were the first instabilities to be found (Lessen, Singh & Paillet 1974) and are known to be present for swirl strength $0 < q < 2.31$ (Stewartson & Brown 1985; Heaton 2007). At their strongest, the inviscid modes are very unstable, but since they are restricted to $q < 2.31$, and indeed they are very weak for $q > 1.6$ (Heaton 2007), they cannot explain instability when $q \geqslant 2$.

(b) Exponential instability modes of a viscous nature (meaning that the exponential growth rate decreases to zero as $Re \to \infty$). This type of instability was first discovered

for rotating pipe flow by Stewartson, Ng & Brown (1988) and was computed in the Batchelor vortex by Khorrami (1991) and Fabre & Jacquin (2004). Khorrami's modes are very weak and restricted to $0 < q < 1.3$, so are not relevant here. Fabre & Jacquin's modes are stronger and can exist for all values of q (Le Dizès & Fabre 2007), so they are a candidate instability mechanism when $q \geqslant 2$. These modes are still relatively weak however, with typical growth rates of 10^{-2} or less, so the magnitude of their contribution is unclear.

(c) Algebraic inviscid instability. This is a weaker instability first found by Heaton & Peake (2006) which can affect vortices when $Re = \infty$. When $Re < \infty$, the algebraic growth is asymptotically damped but translates into transient growth, in the same way that the inviscid lift-up effect translates into transient growth in viscous shear flow (Schmid & Henningson 2001). If sufficiently strong, these transients might offer a 'bypass' route to vortex instability. The mechanism for this inviscid-type transient growth was presented by Heaton & Peake (2007), who found a precise analogy with the well-known transient growth in plane shear flows, both being vestiges of the inviscid continuous spectrum (CS). This effect is present for all values of q.

In this paper, we use optimal growth (see Schmid 2007) to quantify the competition between mechanisms (b) and (c) when $q \geqslant 2$. Optimal growth is especially suited to flows which are asymptotically stable (in the limit $t \to \infty$) or only weakly unstable, and so it is a natural tool for the present problem. The usual procedure of finding the maximum possible growth of disturbances over a specified time interval gives an impartial measure of the scope for instability, and will reveal which mechanisms are used.

Heaton & Peake (2007) described inviscid-type transient growth in general vortices and identified an analogy to the transient growth of streamwise streaks in plane shear flows, as both are derived from algebraic CS instabilities present only when $Re = \infty$. They computed these transients for the Batchelor vortex, restricted to parameter values for which viscous modes are absent, and found that the growth mechanism (c) alone can be a strong effect. As Le Dizès & Fabre (2007) note, viscous modes have some resemblance to the Tollmien–Schlichting waves of a Blasius boundary layer in their mathematical structure (large-Re WKB) and also in the strength of their growth rates. In this paper, we will consider parameters for which effects (b) and (c) are simultaneously present. We will discuss the competition between (b) and (c) and connect two different regimes, one dominated by inviscid transients over short time intervals and a second dominated by viscous modes over long time intervals. The nature of the transition between the two regimes shows that the viscous modes are more likely to be important than the Tollmien–Schlichting waves in a boundary layer, but that the inviscid effects are still likely to be the most important ingredient.

The remainder of this paper is organized as follows. In § 2, we present the governing linearized equations and the numerical method used to calculate optimal gain. In §§ 3 and § 4, we present the main results, and in § 5, we discuss the implications of our results and conclude.

2. Governing equations and numerical method

We work in cylindrical polar coordinates (x, r, θ) with corresponding velocity components (u, v, w). Lengths are scaled on the vortex core radius and velocities are scaled on the vortex swirl. The mean flow is the Batchelor vortex (Batchelor 1964), given by

$$U(r) = q^{-1}\mathrm{e}^{-r^2}, \quad V(r) = 0, \quad W(r) = (1 - \mathrm{e}^{-r^2})/r. \tag{2.1}$$

Note that Fabre & Jacquin (2004) (and others) choose to scale velocities on the vortex axial velocity. Our scales for velocity, and hence also the time coordinate, differ from theirs by a factor of q. We use a 'vortex Reynolds number' Re defined by the mean flow circulation (at infinity) divided by viscosity. Small perturbations $\boldsymbol{u}$, p to the mean velocity and pressure are introduced with constant axial and azimuthal wavenumbers k and m, respectively, so that

$$\boldsymbol{u} = \boldsymbol{u}(r,t)\exp(\mathrm{i}kx + \mathrm{i}m\theta), \quad p = p(r,t)\exp(\mathrm{i}kx + \mathrm{i}m\theta). \tag{2.2}$$

The dynamics are governed by the linearized Navier-Stokes equations

$$\frac{\partial u}{\partial t} + P\mathrm{i}u + vU' = -\mathrm{i}kp + \frac{2\pi}{Re}\left[\frac{(ru')'}{r} - \left(\frac{m^2}{r^2} + k^2\right)u\right], \tag{2.3}$$

$$\frac{\partial v}{\partial t} + P\mathrm{i}v - \frac{2Ww}{r} = -p' + \frac{2\pi}{Re}\left[\frac{(rv')'}{r} - \left(\frac{1+m^2}{r^2} + k^2\right)v - \frac{2\mathrm{i}mw}{r^2}\right], \tag{2.4}$$

$$\frac{\partial w}{\partial t} + P\mathrm{i}w + \frac{(Wr)'v}{r} = -\frac{\mathrm{i}mp}{r} + \frac{2\pi}{Re}\left[\frac{(rw')'}{r} - \left(\frac{1+m^2}{r^2} + k^2\right)w + \frac{2\mathrm{i}mv}{r^2}\right], \tag{2.5}$$

$$0 = \mathrm{i}ku + \frac{(rv)'}{r} + \frac{\mathrm{i}mw}{r}, \tag{2.6}$$

where we have defined $P = Wm/r + Uk$. Boundary conditions for (2.3)–(2.6) are decay at infinity and the appropriate kinematic conditions at $r = 0$ (see Khorrami, Malik & Ash 1989).

The kinetic energy of the disturbance is

$$E(t) = \frac{1}{2}\int_0^\infty (|u|^2 + |v|^2 + |w|^2)\, r\,\mathrm{d}r, \tag{2.7}$$

which is the norm we use to measure the strength of the disturbance. Using the standard terminology we refer to $E(t)/E(0)$ as the energy amplification of an initial condition at time t. Choosing a fixed time $t = \tau$, the gain $G(\tau)$ is defined as the maximum energy amplification at time τ, the maximum being taken over all permissible initial conditions. The disturbance which attains the maximum energy gain is referred to as the optimal disturbance for that τ, e.g. 'the $\tau = 50$ optimal disturbance'. For stable flows $G_{max} \equiv \max_\tau G(\tau)$ can be defined, and is usually the principal measure of optimal growth levels. Here, however, our interest is in an unstable region of parameter space where G_{max} is undefined, so we deal directly with the gain $G(\tau)$ itself. In order to compute the gain we first discretize the spatial radial coordinate using a pseudospectral collocation technique, mapping the interval $0 \leqslant r \leqslant \infty$ onto $-1 \leqslant \xi \leqslant 1$ by the transformation $\xi = (r-1)/(r+1)$. Using this discretization, with N collocation points, equations (2.3)–(2.6) transform into a $(4N \times 4N)$ matrix equation. The gain is then calculated using the method described fully in Schmid & Henningson (2001, chap. 4). This involves finding the frequency eigenvalues and eigenvectors of (2.3)–(2.6), by solving the eigenvalue problem in the discretized matrix form of the equations. After this the matrix equation is diagonalized and the optimal gain can be computed as a norm of the matrix exponential, where the appropriate norm is dictated by (2.7); see Schmid & Henningson (2001, chap. 4) for full details. We use MATLAB$^{\mathrm{TM}}$ to perform the linear algebra on a standard desktop computer. The rate-limiting step in the procedure is the eigenvalue–eigenvector calculation, which has $O(N^3)$ complexity. Our code is validated in two ways, first the eigenvalue spectrum has been compared to the results of Fabre & Jacquin (2004) to check the spatial

discretization, and secondly, the gain $G(\tau)$ has been checked against the results of Heaton & Peake (2007) (who used a different method to calculate the gain).

3. Gain curve results

3.1. *Topography of the instabilities*

Our interest is in the Batchelor vortex when the swirl strength $q \geqslant 2$ and the Reynolds number Re is large. As mentioned in § 1, there are no strong instabilities in this regime of the mean flow, but there are two relatively weak growth processes available. One process is weak exponential growth by the viscous modes of Fabre & Jacquin (2004). These modes exist at sufficiently large Re for wavenumbers satisfying

$$0 < k < -m/q, \quad m < 0, \tag{3.1}$$

(see Fabre & Jacquin 2004; Le Dizès & Fabre 2007).

The second growth process available is algebraic transient growth, which uses the inviscid CS, as explored by Heaton & Peake (2007). The mechanism for the underlying algebraic instability is vortex stretching of disturbances by the sheared mean flow (Heaton & Peake 2006). The mechanism for the optimal transient behaviour is analogous to that in two-dimensional shear flow, in particular to the oblique modes in two-dimensional shear flow (Heaton & Peake 2007, § 4) because all modes are necessarily oblique in a swirling jet. As a result, the transients differ slightly from the streamwise modes and 'lift-up effect' familiar in two-dimensional shear flow (Landahl 1980), and from the axisymmetric modes and 'anti-lift-up effect' recently discovered in vortices without a jet component (Antkowiak & Brancher 2007). The inviscid transients have $G(\tau) \sim \tau^{2+2\sigma_{max}}$ for $1 \ll \tau \ll t_{visc}$ and subsequently are damped for $\tau \geqslant t_{visc}$, where $t_{visc} = Re^{1/3}$ is the relevant time scale of viscous damping. Transient growth is possible via this process for all k, m, but for wavenumbers not satisfying (3.1) it is found that $\sigma_{max} = 0$ (Heaton & Peake 2007) and the effect is weak. Wavenumbers k, m which do satisfy (3.1) have $\sigma_{max} = \infty$. This means formally that gain $G(\tau)$ faster than any power of τ occurs via inviscid processes for $1 \ll \tau \ll t_{visc}$ before being asymptotically damped, implying stronger transient growth.

The two competing growth mechanisms therefore coexist in the same region of parameter space, which for each $m < 0$ is given by (3.1) as a portion of the (q, k)-plane. The balance between the two mechanisms is intricate, and depends on the parameters at hand. In the limit of $Re \to \infty$, the CS driven transient growth must dominate for all τ and all k, m. This is because the growth rate of the primary viscous modes decays as $Re^{-1/3}$, while the CS transient growth approaches its inviscid limit. Similarly, for Re less than the critical value for unstable viscous modes (the critical value of Re depends on q, k and m, but is typically of order 10^4, see Fabre & Jacquin 2004), the CS transient growth must dominate. This latter regime, in which the viscous modes are damped, was used for the demonstration of CS transient growth given by Heaton & Peake (2007). Between the two regimes described is a wide range of large, but finite, Re for which the balance of the two growth processes is not clear: this is the range we consider here. This range of Re is not unrealistically high, Fabre & Jacquin (2004) estimate $Re \simeq 10^5$ for a large aeroplane, so this delicate mathematical balance will indeed be present at physically relevant parameters.

3.2. *Calculated gain for* $m = -1$

Our interest in values of Re above the critical value for viscous modes means that the flow is asymptotically unstable. The long-time exponential growth of the viscous

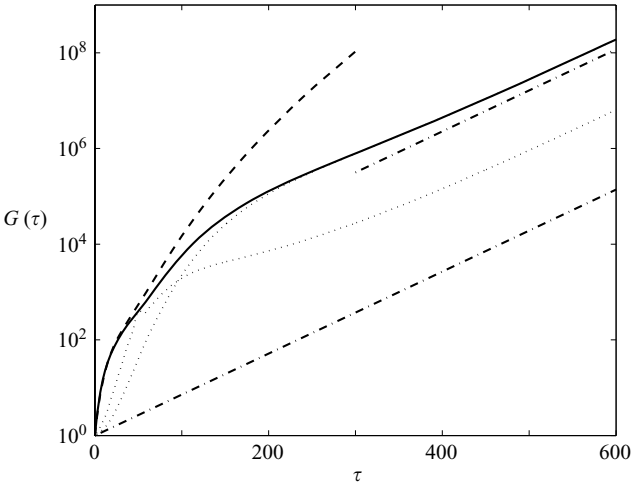

FIGURE 1. Gain curve at $q=2$, $m=-1$, $k=0.268$ and $Re=1.74\times10^5$. The solid line shows $G(\tau)$. The dashed line shows $G_{inv}(\tau)$, i.e. the gain curve when $Re=\infty$ but q, m, k are unchanged. The dash-dot lines indicate the growth rate of the primary viscous mode. The dotted lines show the energy amplification curves for the $\tau=50$ and $\tau=500$ optimals.

modes, albeit relatively weak, means that $G_{max}(\equiv \max_\tau G(\tau))$, which is usually the principal quantity for measuring growth levels, is undefined. Instead, as intimated in § 2, we will have to inspect the entire gain curve $G(\tau)$ in this investigation. Another factor which complicates the interpretation of numerical results is that, as explained in § 3.1, the two effects inhabit exactly the same range of wavenumbers (3.1). In two-dimensional channel and boundary-layer flows, the corresponding effects are well-separated in wavenumber space: If α, β denote the streamwise and spanwise wavenumbers, then the weak exponential instabilities (the Poiseuille flow instability mode or Tollmien–Schlichting waves) are strongest at $\beta=0$ (by Squire's theorem, see Drazin & Reid 1981). On the other hand, the strongest CS derived transient growth occurs at $\alpha=0$, where viscous damping of the inviscid CS is weakest (because $t_{visc}=Re$ for $\alpha=0$ and $t_{visc}=Re^{1/3}$ for $\alpha\neq0$, see Chapman 2002; Heaton & Peake 2007). This separation in wavenumber space leads to two distinct local maxima of the gain in the (α,β)-plane and consequently a clear-cut transition between the two effects: at early times, the $\alpha=0$ CS transient growth is strongest, but at a certain time the local maximum with $\beta=0$ overtakes it, and for all subsequent times the instability mode provides the strongest growth. Figure 7 of Corbett & Bottaro (2000) gives a clear illustration of this. Here the two effects are simultaneously present in the Batchelor vortex for the same wavenumbers (3.1), which will cause the transition between the two regimes to be of a more gradual nature.

Gain curves have been calculated as outlined in § 2, and an example of the shape of the gain curve we find is shown in figure 1. In figure 1, we assume $q=2$ to determine the mean flow. At larger q, the viscous modes are both weaker and reliant on higher values of Re (Fabre & Jacquin 2004, figure 4). The CS transient growth is anticipated to have approximately the same strength for larger q (Heaton & Peake 2007, figure 8*b*), therefore we choose $q=2$ in the first instance to give a fair comparison of the two effects. Taking $q=2$ and $m=-1$, the values of $k=0.268$ and $Re=1.74\times10^5$ were both chosen to maximize the growth rate of the primary viscous mode, which we find to be $\mathrm{Im}(\omega)=9.87\times10^{-3}$. These values are in agreement with the viscous mode

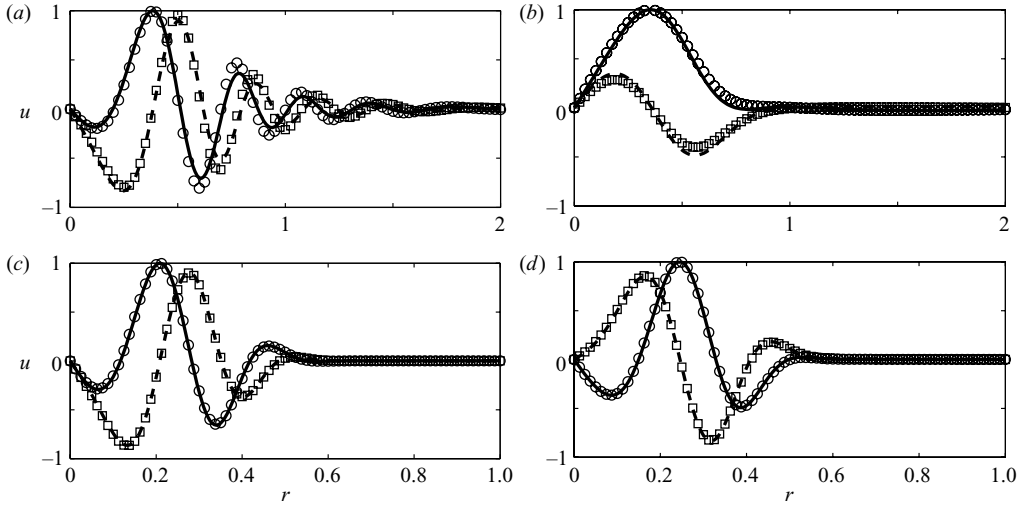

FIGURE 2. Optimal disturbances for the parameters in figure 1. Solid and dashed lines show the real and imaginary part of u for the $\tau = 50$ optimal (a, b) and the $\tau = 500$ optimal (c, d). (a, c) show the initial disturbance $u(t = 0)$, while (b, d) show the final disturbance $u(t = \tau)$. The symbols are for comparison, and are explained in the text.

calculations of Fabre & Jacquin (2004), in particular see their figures 4(a) and 5. For the comparison, note that our definition of the Reynolds number differs from theirs by a factor of $2\pi q$, and that our time scale differs from theirs by a factor of q. All disturbances must asymptotically grow with this exponential growth rate at long times, for example see the $\tau = 50$ and $\tau = 500$ optimals in figure 1. In what follows, we discuss the behaviour seen at finite times.

Figure 1 shows that for $0 \leqslant \tau \leqslant 100$, the gain curve initially follows the growth possible for an inviscid vortex with the same corresponding parameters (shown by the dashed line). This suggests that the early growth is being attained via the transient CS mechanism, and that viscosity therefore is having a stabilizing effect on the optimal perturbation. At later times such as $\tau \geqslant 400$, the gain curve is approximately linear in figure 1, corresponding to exponential growth of $G(\tau)$. The gradient of the dash-dot straight lines indicates the rate of growth of the primary viscous mode, and it is seen that $G(\tau)$ approaches this gradient for larger τ. This suggests that for larger τ the optimal growth is attained via the viscous mode, a portion of the spectrum on which viscosity has a destabilizing action. While the shape of the gain curve in figure 1 is highly suggestive, in order to confirm these suspected mechanisms we examine the nature of the optimal disturbances in more detail in figure 2.

Figure 2 shows the axial component u of the optimal disturbances for $\tau = 50$ (figure 2a, b) and $\tau = 500$ (figure 2c, d). Figures 2(a) and 2(c) show the optimal initial conditions at $t = 0$ and figures 2(b) and 2(d) show the optimal disturbance (which evolves according to (2.3)–(2.6)) at time $t = \tau$. We display only u for simplicity, similar behaviour is observed for the other components v, w, p of the disturbances. Note also that in figures 2(b) and 2(d), u is rescaled to have unit norm to allow comparison, but in reality the disturbances grow in magnitude such that $G(50) = 391$ and $G(500) = 2.78 \times 10^7$. The $\tau = 50$ optimal is suggested to use the CS transient mechanism discussed by Heaton & Peake (2007). Optimal disturbances using the CS mechanism contrive to arrange efficient cancellations of the various CS eigenfunctions

in the initial ($t=0$) data, see Appendix B of Heaton & Peake (2007) for full details, leading to initial data which are characteristically very oscillatory. As CS optimals evolve towards $t=\tau$, the cancellations present in the initial data evaporate, because of differences in the complex phase for the different frequencies of the CS. The optimal disturbance best exploits this mechanism, and therefore has very little cancellation present when $t=\tau$ and is characteristically not oscillatory. This behaviour is recognized in the $\tau=50$ optimal by the oscillatory initial data (figure 2*a*) and the markedly simpler structure of the data at $t=\tau=50$ (figure 2*b*). Final confirmation of the mechanism is given by comparing the optimal disturbance with the symbols in figures 2(*a*) and 2(*b*), which represent the optimal disturbance for the same parameters in a purely inviscid vortex. After the optimal time, since there are no more cancellations in the disturbance field, the inviscid mechanism is spent; the disturbance, in general, possesses a component of the viscous mode, and this must provide the subsequent growth. The energy amplification curve $E(t)/E(0)$ for the $\tau=50$ optimal is shown by a dotted line in figure 1: correspondingly, it shows initially rapid growth but after $t=50$ subsequently settles down to the slower growth rate of the viscous mode.

Figures 2(*c*) and 2(*d*) show the $\tau=500$ optimal disturbance, which it is suggested relies on the primary viscous mode to attain its energy growth. It is immediately clear from the nature of the initial data (note the different scales on the axes) that the $\tau=500$ optimal has a very different structure to the $\tau=50$ optimal. The optimal growth for a non-normal operator possessing a primary unstable eigenmode ϕ_1, in the absence of alternative mechanisms, is attained by the primary adjoint eigenmode ψ_1 (see Corbett & Bottaro 2000; Chomaz 2005). If the $\tau=500$ optimal is dictated by the primary viscous mode, we would expect the initial condition to resemble ψ_1 (the adjoint eigenmode) and the disturbance later to resemble ϕ_1 (the proper eigenmode). In figures 2(*c*) and 2(*d*), the adjoint and proper eigenmodes, respectively, are plotted for comparison using the symbols. The excellent agreement of the symbols with the computed lines confirms that the $\tau=500$ optimal indeed has straightforward optimal growth of the primary viscous instability mode. The energy amplification curve $E(t)/E(0)$ is shown by a dotted line in figure 1. All optimals in the large-τ regime share the same initial condition (ψ_1), and so they also closely follow the same energy amplification curve.

The trend observed in figure 1, and confirmed using figure 2, is of optimal growth at smaller τ dominated by CS transients, followed by a regime at larger τ dominated by the primary viscous mode. This is the same trend seen in a two-dimensional boundary layer (Corbett & Bottaro 2000) and the explanation is similar. The CS transient growth is typically algebraic in nature (see § 4 of Heaton & Peake 2007). For smaller τ, algebraic growth exceeds a weak exponential instability $\exp(\sigma\tau)$ with small growth rate (recall σ is of order 10^{-2} for a viscous mode, or 10^{-3} for a Tollmien–Schlichting wave). For larger τ, the exponential must eventually surpass the algebraic growth, causing the transition to a second regime at larger τ. Between the two distinct regimes examined at $\tau=50$ and 500 in figure 2, we observe a smooth transition of the gain curve in figure 1. The balance between the two mechanisms in the transition region is visible in the form of the optimal disturbances for intermediate τ. As τ increases, we find that the initial condition in figure 2(*a*) gradually migrates towards smaller r and the size of the oscillations at the larger r gradually decreases. At $\tau=200$, the initial optimal is similar in shape to ψ_1, the adjoint eigenmode in figure 2(*c*), however it still extends to larger r than ψ_1 and still contains some small oscillations beyond those present in ψ_1. This indicates that at $\tau=200$, in the transition region, both

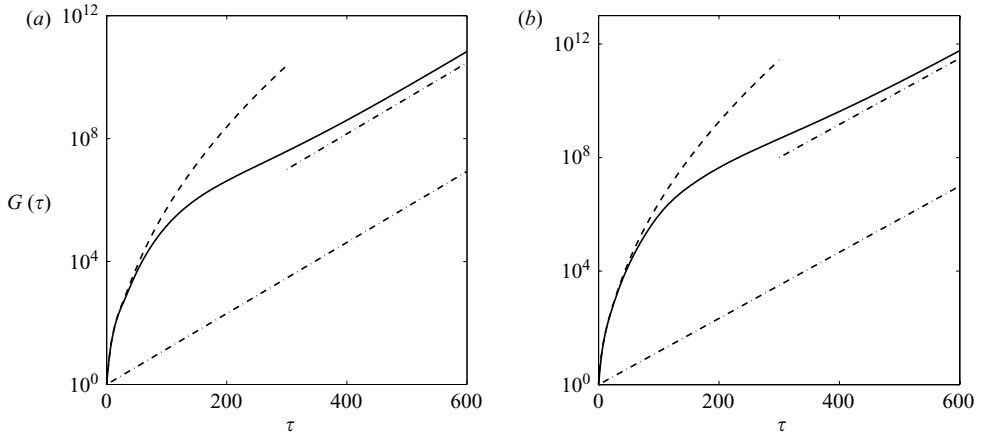

FIGURE 3. Gain curves at $q = 2$ for (*a*) $(m, k, Re) = (-2, 0.552, 3.02 \times 10^5)$ and (*b*) $(m, k, Re) = (-3, 0.845, 6.76 \times 10^5)$. Curves have the same meaning as in figure 1.

mechanisms are still contributing. This smoothness of the transition is not necessarily expected in a quantity defined by an optimization, and certainly contrasts sharply with the corresponding picture in a Blasius boundary layer (figure 7 of Corbett & Bottaro 2000). For $\tau > 200$, the gain $G(\tau)$ and the energy amplification of the large-τ optimals are almost equal, indicating that the transition region ends at about this point.

3.3. *Gain levels for* $m \leqslant -2$

A detailed discussion has been given of the $m = -1$ case, and similar behaviour was also observed for $m = -2, -3$. For these values, the gain curves are shown in figure 3, where again we have taken $q = 2$ and choose k and Re in order to maximize the growth rate of the primary viscous mode. Figure 3 shows the same trends as figure 1, and we find that the same type of transition occurs between a regime dominated by inviscid CS transients and a regime dominated by the primary viscous mode.

One difference to note is that the gain levels are somewhat higher in figure 3 than figure 1, this is partly due to the higher values of Re in the plots as well as the variation of m. Figure 4 shows a comparison of optimal growth levels across various wavenumbers for fixed q and Re, the values taken being those used in figure 1. Figure 4 shows the comparison for $\tau = 50$, 200 and 500, corresponding to the inviscid, transition and viscous regimes of figure 1, respectively. In each regime, the gain is found to be greatest for finite $|m|$: the inviscid gain $G_{inv}(\tau)$ (the dashed lines in figures 1 and 3) increases with $|m|$; however, at larger $|m|$, inviscid mechanisms are more strongly damped by viscosity (e.g. see Denier & Stott 2005). This balance causes the inviscid transients to reach a maximum at $m = -3$ in figure 4(*a*). In the viscous regime, it is the growth rate of the primary mode which counts, and this too is maximum at finite $|m|$. In this case, $m = -2$ has the greatest growth rate (see figure 4*a* of Fabre & Jacquin 2004, and recall that we use the Re maximizing the $m = -1$ growth rate), and correspondingly $m = -2$ has the greatest gain in figure 4(*c*) when $\tau = 500$. For $m \leqslant -5$, all viscous modes are stable in this case, implying much smaller growth at large τ (figure 4*c*). Note that for these modes, the gain increases weakly with k, which is unexpected at first because increasing k is usually associated with increased viscous damping. Viscous modes, however, are destabilized by viscosity and in fact this trend reflects a weak increase in $\mathrm{Im}(\omega)$ for the least-damped viscous mode as

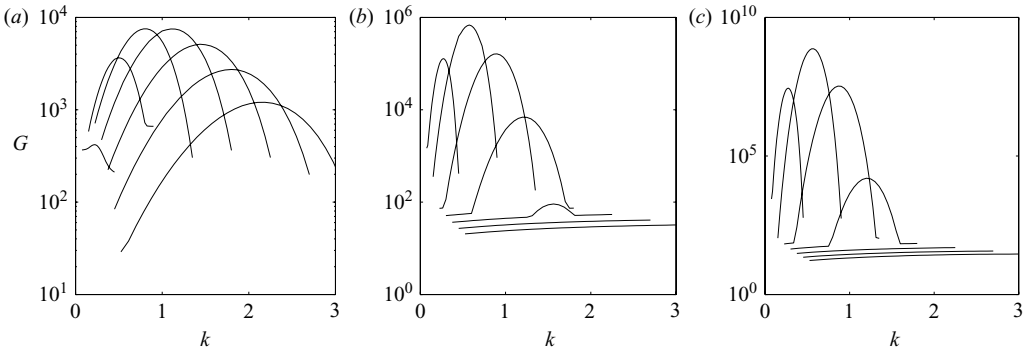

FIGURE 4. Gain $G(\tau)$ for $Re = 1.74 \times 10^5$, $q = 2$ at (*a*) $\tau = 50$, (*b*) $\tau = 200$, (*c*) $\tau = 500$. In each case the seven curves from left to right correspond to $m = -1, -2, \ldots, -7$ (so that the $m = -1$ curve is the narrowest and covers the smallest range of k, the $m = -7$ curve is the widest).

k increases. This is observed numerically in our calculations, and is explained by equation (5.5) of Le Dizès & Fabre (2007).

4. The inviscid gain curve as $\tau \to \infty$

An interesting question surrounds the precise nature of the inviscid (dashed) lines in figures 1 and 3. When there is no exponentially growing unstable eigenvalue in the inviscid equations, we expect inviscid gain $G_{inv}(\tau) \sim \tau^{2+2\sigma_{max}}$ as $\tau \to \infty$, where σ_{max} is the maximum exponent of the algebraic CS instability. Heaton & Peake (2007) verified this scaling in cases with finite σ_{max}, but for the Batchelor vortex the precise scaling is unclear because $\sigma_{max} = \infty$ and $G_{inv}(\tau)$ increases faster than any power of τ. Investigation of $G_{inv}(\tau)$ using our present numerical method appears to indicate a scaling of the type $G_{inv}(\tau) \sim \exp(\tau^{1/2})$ in the $\tau \to \infty$ asymptotic limit. Our numerical computations reach their limit at $\tau \simeq 500$ owing to round-off errors and larger values of τ are required in order to fully confirm the scaling, but an $\exp(\tau^{1/2})$ shape is consistently found and is sufficiently unusual to merit a mention. We note that a precedence does exist for linear operators to have exponential gain, even though they do not possess an unstable eigenvalue (see Trefethen 1997, which discusses two such operators due to Zabczyk and Hille & Phillips). Such behaviour has not been encountered in a fluid dynamics context, so it would be interesting to confirm any such structure in the linearized Navier–Stokes equations.

The results of § 3 clearly indicate that for large τ the optimal gain is controlled by the primary viscous mode and the inviscid theory is not relevant. Nevertheless, we highlight the unusual scaling $G_{inv}(\tau) \sim \exp(\tau^{1/2})$ as $\tau \to \infty$ which our limited numerical evidence suggests, as there may be other circumstances in which it is relevant.

5. Conclusions

The present results attempt to establish the significance of Fabre & Jacquin's viscous modes in the context of the initial-value problem for instability of a trailing vortex. We have used optimal growth in an attempt to measure impartially the strength of the viscous instabilities and their competition with inviscid natured transients. Attention has been restricted to mean flows with $q \geqslant 2$ in which these two are the

only known growth mechanisms, both of which can be described as relatively weak. The competition between inviscid transients and viscous modes described in this paper is expected to be mirrored in all other non-trivial vortices (as both growth mechanisms are generic). While the Batchelor vortex may be criticized as a model of reality (Spalart 1998), it is a useful prototype, not least because there is a large literature detailing the parameters for which each linear instability applies.

We find a transition between two distinct regimes. Over short time intervals, the strongest growth is solely due to inviscid CS transients, whereas over longer intervals the optimal growth is solely due to the primary viscous mode. A helpful analogy exists with the linear growth of disturbances to a Blasius boundary layer, where the weak instability modes are Tollmien–Schlichting waves and the inviscid CS transients are streamwise independent structures. In a Blasius boundary layer, the optimal disturbances for the two mechanisms have very different wavelengths, and the transition between the two regimes is sharp (for times shorter than a critical value, all optimals are exclusively streamwise-independent transients, whereas for times longer than the critical value, the optimal is just the Tollmien–Schlichting wave, see Corbett & Bottaro 2000). Here, in contrast, the two mechanisms use the same wavelengths and have more similar optimal disturbances. A smooth transition is found in which, over intermediate time intervals, the optimal disturbance uses both mechanisms to contribute to its energy growth. The balance between inviscid transients and viscous modes is therefore more evenly balanced than in a boundary layer. The reasons for this are the wavelengths of the optimal disturbances, the viscous mode growth rates (which are a little larger than Tollmien–Schlichting growth rates) and the viscous damping time scale for the inviscid transients ($t_{visc} = Re^{1/3}$ here, whereas $t_{visc} = Re$ in a boundary layer, Heaton & Peake 2007). These factors appear able to compensate for the extra strength of the inviscid transients themselves ($\sigma_{max} = \infty$ in the Batchelor vortex whereas $\sigma_{max} = 0$ in boundary layers and two-dimensional shear flows), at least in the cases considered here. It should be recalled that the values of q, Re used in figures 1 and 3 were chosen to maximize the strength of the primary viscous mode, so there are also many values for which the viscous modes are less significant.

We have found the optimal linear gain $G(\tau)$ to be a useful measure of instability for the comparisons made in this paper, but it does have limitations, in particular to realize the gain requires a very specialized disturbance. It is widely believed that strong gain is an indication of strong growth from stochastic processes (Schmid 2007), which is perhaps a more realistic scenario in practice. Indeed, optimal growth has strong links to instability from random forcing (Farrell & Ioannou 1993), and also to random uncertainties in the mean-flow operator itself (Trefethen 1997), each of which may be effects of free-stream turbulence in reality.

Further, optimal linear growth does not measure the nonlinear importance of a linear growth mechanism. Determining which disturbances (in particular which values of m) best seed nonlinear instability of the vortex requires a different analysis, although we may reasonably expect the linear results to offer some indication. Also, the time at which nonlinear effects become significant cannot be concluded from our linear analysis. When the viscous regime becomes dominant, the gain is already very high, so it is not clear that linear theory can access the large-τ regime. If it cannot, because the growth possible in the inviscid regime is sufficient to invoke nonlinearity, then this would imply a bypass route to instability. For the trailing line vortex application, a first indication may be obtained by attempting to translate our temporal results into spatial results. Following the scaling arguments of Fabre & Jacquin (2004), in turn based on the experimental results of Jacquin *et al.* (2001), we obtain an order of

magnitude estimate that $\tau = 500$ corresponds to roughly 25 wing spans downstream of an aircraft. This value is comparable to the characteristic scale of the Crow instability, which would suggest an aircraft vortex is unlikely to experience much of the large-τ regime before other effects, neglected here, become important. The transition region between the regimes, at about $\tau = 200$ or 10 wing spans downstream, might however be accessible.

The author thanks Trinity College, Cambridge, for its financial support.

REFERENCES

Antkowiak, A. & Brancher, P. 2007 On vortex rings around vortices: an optimal mechanism. *J. Fluid Mech.* **578**, 295–304.

Batchelor, G. K. 1964 Axial flow in trailing line vortices. *J. Fluid Mech.* **20**, 645–658.

Chapman, S. J. 2002 Subcritical transition in channel flows. *J. Fluid Mech.* **451**, 35–97.

Chomaz, J. M. 2005 Global instabilities in spatially developing flows: non-normality and nonlinearity. *Annu. Rev. Fluid Mech.* **37**, 357–392.

Corbett, P. & Bottaro, A. 2000 Optimal perturbations for boundary layers subject to stream-wise pressure gradient. *Phys Fluids* **12** (1), 120–130.

Denier, J. P. & Stott, J. A. K. 2005 The dominant wave mode within a trailing line vortex. *Phys Fluids* **17**, 014101.

Drazin, P. G. & Reid, W. H. 1981 *Hydrodynamic Stability*. Cambridge University Press.

Fabre, D. & Jacquin, L. 2004 Viscous instabilities in trailing vortices at large swirl number. *J. Fluid Mech.* **500**, 239–262.

Farrell, B. F. & Ioannou, P. J. 1993 Stochastic forcing of the linearized Navier-Stokes equations. *Phys Fluids* A **5** (11), 2600–2609.

Heaton, C. J. 2007 Centre modes in inviscid swirling flows and their application to the stability of the Batchelor vortex. *J. Fluid Mech.* **576**, 325–348.

Heaton, C. J. & Peake, N. 2006 Algebraic and exponential instability of inviscid swirling flow. *J. Fluid Mech.* **565**, 279–318.

Heaton, C. J. & Peake, N. 2007 Transient growth in vortices with axial flow. *J. Fluid Mech.* **587**, 271–301.

Jacquin, L., Fabre, D., Geffroy, P. & Coustols, E. 2001 The properties of a transport aircraft wake in the extended nearfield: an experimental study. *AIAA Paper* 2001-1038.

Khorrami, M. R. 1991 On the viscous modes of instability of a trailing line vortex. *J. Fluid Mech.* **225**, 197–212.

Khorrami, M. R., Malik, M. R. & Ash, R. L. 1989 Application of spectral collocation techniques to the stability of swirling flows. *J. Comput. Phys.* **81**, 206–229.

Landahl, M. T. 1980 A note on an algebraic instability of inviscid parallel shear flows. *J. Fluid Mech.* **98**, 243–251.

Le Dizès, S. & Fabre, D. 2007 Large-Reynolds-number asymptotic analysis of viscous centre modes in vortices. *J. Fluid Mech.* **585**, 153–180.

Leibovich, S. 1978 The structure of vortex breakdown. *Annu. Rev. Fluid Mech.* **10**, 221–246.

Lessen, M., Singh, P. J. & Paillet, F. 1974 The stability of a trailing line vortex. Part 1. Inviscid theory. *J. Fluid Mech.* **63**, 753–763.

Schmid, P. J. 2007 Nonmodal stability theory. *Annu. Rev. Fluid Mech.* **39**, 129–162.

Schmid, P. J. & Henningson, D. S. 2001 *Stability and Transition in Shear Flows*. Springer.

Spalart, P. R. 1998 Airplane trailing vortices. *Annu. Rev. Fluid Mech.* **30**, 107–138.

Stewartson, K. & Brown, S. N. 1985 Near-neutral centre-modes as inviscid perturbations to a trailing line vortex. *J. Fluid Mech.* **156**, 387–399.

Stewartson, K., Ng, T. W. & Brown, S. N. 1988 Viscous centre modes in the stability of swirling Poiseuille flow. *Phil. Trans R. Soc. Lond.* A **324**, 473–512.

Trefethen, L. N. 1997 Pseudospectra of linear operators. *SIAM Rev.* **39**, 383–406.